

Traveling waves of activity in primary visual cortex during binocular rivalry

Sang-Hun Lee^{1,3}, Randolph Blake² & David J Heeger¹

When the two eyes view large, dissimilar patterns that induce binocular rivalry, alternating waves of visibility are experienced as one pattern sweeps the other out of conscious awareness. Here we combine psychophysics with functional magnetic resonance imaging to show tight linkage between dynamics of perceptual waves during rivalry and neural events in human primary visual cortex (V1).

The cortex is an excitable medium through which waves of neural activity can propagate^{1,2}. Binocular rivalry, the perceptual alternations induced when incompatible patterns are presented to the two eyes, provides a rare opportunity to observe the perceptual concomitants of neural wave propagation³. During an alternation, one sees a traveling wave in which the dominance of one pattern emerges locally and expands progressively as it renders the other pattern invisible⁴. Several converging lines of evidence have suggested that primary visual cortex (V1) may be involved in the spatiotemporal dynamics of these perceptual traveling waves, but that involvement had not, so far, been demonstrated. Here we use functional magnetic resonance imaging (fMRI) to measure and characterize traveling waves of cortical activity during binocular rivalry.

Human observers viewed a dichoptic display designed to induce perceptual waves (Fig. 1a). Experiments were carried out with the written

consent of each observer, and in compliance with the safety guidelines for MRI research, as approved by the Stanford University Panel on Human Subjects in Medical Research. The rival images were a low-contrast radial grating (viewed by one eye) and a high-contrast spiral grating (viewed by the other eye), each restricted to an annular region of the visual field centered on the point of fixation. Exploiting the susceptibility of binocular rivalry to transient stimulation⁵, we triggered shifts in perceptual dominance through a brief, abrupt increase in contrast in a small region of the low-contrast grating at the top of the annulus (see **Supplementary Methods** and **Supplementary Fig. 1** online). This contrast pulse typically evoked a perceptual traveling wave, so that observers perceived the local dominance of the low-contrast image as spreading around the annular region, starting at the top of the annulus and progressively erasing the high-contrast image from visual awareness⁴ (**Supplementary Video 1** online). Observers pressed a key when a perceptual wave reached a target area (marked by nonius lines) at the bottom of the annulus. This key press triggered the disappearance of the two monocular gratings until the beginning of the next trial.

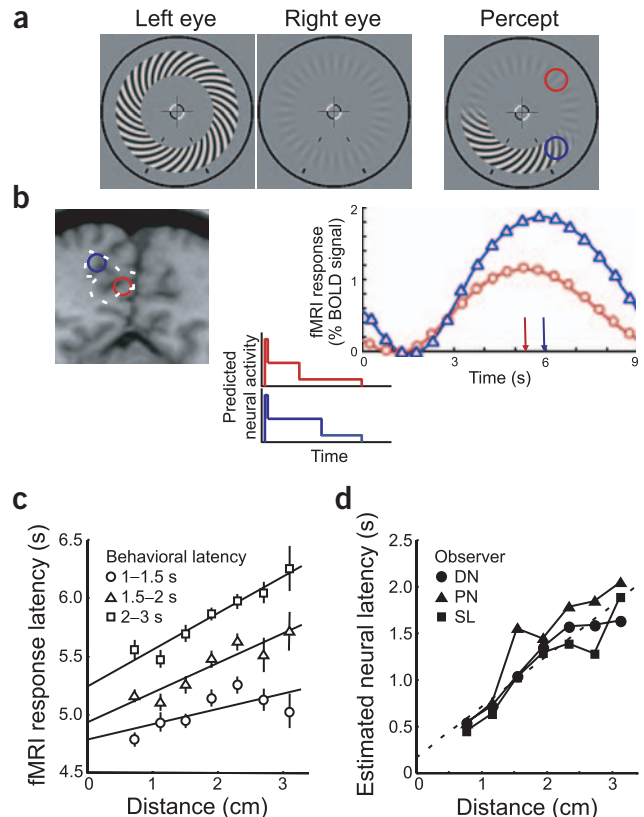


Figure 1 Traveling waves of cortical activity in human V1. **(a)** Left two panels, stimuli were rival gratings viewed dichoptically. Right panel (Percept), snapshot of the perceptual traveling wave in which the low-contrast pattern was seen to spread around the annulus, starting at the top. **(b)** Left, anatomical image passing through the posterior occipital lobe, roughly perpendicular to the calcarine sulcus. Red outline, subregion of V1 corresponding retinotopically to the upper-right quadrant of the stimulus annulus. Blue outline, subregion of V1 corresponding to the lower-right quadrant of the stimulus. Middle, time series of the predicted neural activity according to a simplified model (see **Supplementary Methods** online). Right, time series of the measured fMRI responses corresponding to the two outlined subregions, averaged across ~1,000 trials for one observer. Red and blue arrows, times at which corresponding curves peak. **(c)** Temporal delay in the fMRI responses as a function of cortical distance from the V1 representation of the top of the annulus, categorized by behavioral latency and averaged across observers. Steeper slope corresponds to slower speed. Larger y -intercept corresponds to longer initial delay. Error bars, s.e.m. **(d)** Estimated propagation speed of the underlying neural activity, averaged across behavioral latencies. Dashed line, best fit to the mean across observers.

¹Department of Psychology and Center for Neural Science, New York University, 6 Washington Place, 8th floor, New York, New York 10003, USA. ²Department of Psychology, Vanderbilt University, 512 Wilson Hall, Nashville, Tennessee 37203, USA. ³Present address: Department of Psychology, Seoul National University, Seoul, South Korea. Correspondence should be addressed to D.J.H. (david.heeger@nyu.edu).

If activity in the visual cortex reflects the spatiotemporal dynamics of rivalry, then there should be a wave of cortical activity coincident with the perceptual wave (Fig. 1b). Specifically, the peak of the fMRI responses at locations along the path of the cortical wave should be increasingly delayed with increasing distance from the cortical representation of the top of the annulus. This is because (i) locations further from the point of origin of the traveling wave will respond to the high contrast for longer durations, and (ii) fMRI responses in V1 increase monotonically with stimulus contrast⁶. It is important to keep in mind, however, that the physical contrasts of both rival gratings remained unchanged—only the perceptual transitions associated with rivalry provided the potential conditions for traveling waves of cortical activity.

V1 did indeed show traveling waves of activity while observers experienced perceptual traveling waves (Fig. 1c and Supplementary Video 2 online). Gray matter corresponding to the V1 representation of the stimulus annulus was identified using conventional retinotopic mapping procedures⁷. For each voxel within this subregion of V1 gray matter, we calculated the temporal delay of the fMRI responses averaged across trials (see Supplementary Methods online). The resulting temporal delays increased with distance from the V1 representation of the top of the stimulus annulus. The correlation between temporal delay and cortical distance was statistically significant in each individual observer ($P < 0.05$, Pearson χ^2 test). This occurred despite the absence of wave-like changes in the stimulus itself.

The dynamics of these cortical waves of V1 activity correlated with the latency of the perceptual waves (Fig. 1c). We segregated the trials into three categories based on the latency of the observers' key-press responses and averaged the fMRI data across trials separately for each of the three ranges of behavioral latencies. Both the speed (slope of the line of best fit) and the initial delay (y -intercept) of the cortical waves increased with behavioral latency ($P < 0.0001$, bootstrap statistical test; see Supplementary Methods online for details).

To compare more directly the fMRI data with the perceptual phenomena during rivalry, we estimated the speed of propagation of the underlying cortical activity from the measured fMRI responses (Fig. 1d). This was done using a model of the underlying neural activity (Fig. 1b) along with a model for how an fMRI signal depends on underlying neural activity (see Supplementary Methods online for details). In addition to the unknown neural response latencies, the model had five free parameters: one parameter corresponded to the ratio of the amplitudes of the tonic neural activity for each of the two stimulus contrasts, another characterized the amplitude of transient neural responses evoked by abrupt stimulus onset at the beginning of each trial, and three were used to characterize the hemodynamic impulse response. Values for these five parameters were determined separately for each observer by fitting the model to the fMRI responses evoked by physical traveling waves. In a separate 'replay' experiment, sequences of monocular images were shown to observers, mimicking perceptual waves under nonrivalry conditions. We had complete information about the timing of neural events during this replay experiment; the neural-response amplitudes and the hemodynamic

impulse response were the only parameters that had to be determined, which was done by fitting the fMRI responses to the physical traveling waves. With those five parameters fixed, we then fit the model to the fMRI responses measured during rivalry, which resulted in separate estimates for the latencies of the underlying neural activity for each voxel of V1 gray matter. A linear fit of the neural latencies revealed wave propagation speeds across the three observers of 1.6–2 cm/s; these propagation speeds compare favorably to the speed value of 2.2 cm/s estimated from psychophysical measurements using essentially the same stimulus⁴.

In summary, the time course of cortical activity varied systematically across the retinotopic map in V1, in correspondence with the subjective perception of traveling waves during binocular rivalry. These results go beyond those from previous single-unit electrophysiology^{8–10} and neuroimaging^{11–15} studies by demonstrating that V1 activity reflects the spatiotemporal dynamics of perception during rivalry. Furthermore, the data show that fMRI is capable of resolving timing differences of ~115 ms over a distance of ~3.5 mm (Fig. 1c). It remains to be seen whether these cortical waves originate in V1 via long-range intracortical connections or whether they are evoked by feedback from higher-order visual cortical areas.

Note: Supplementary information is available on the Nature Neuroscience website.

ACKNOWLEDGMENTS

We thank N. Logothetis, C. Koch and the late F. Crick for comments on an earlier version of the manuscript. Supported by grants from the National Institutes of Health to D.J.H. (EY12741) and to R.B. (EY14437), and a grant from the Korea Institute of Science & Technology Evaluation and Planning to S.H.L. (M103KV010021-04K2201-02140). Data were acquired while D.J.H. and S.H.L. were at Stanford University. Part of this work was completed while R.B. was a visiting scholar at New York University.

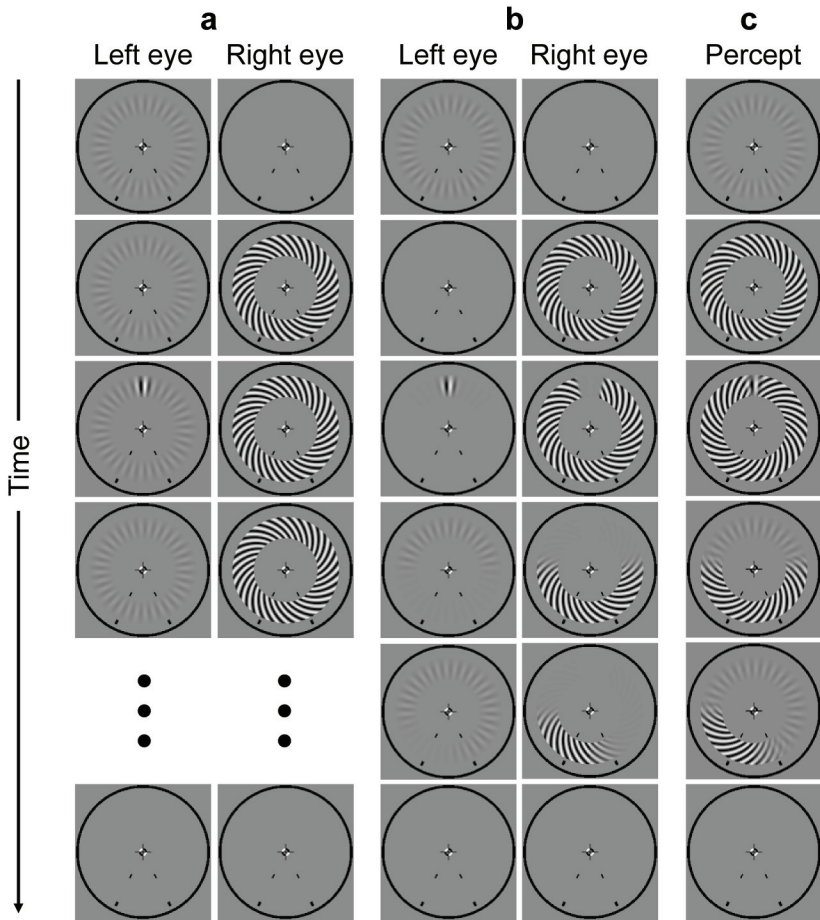
COMPETING INTERESTS STATEMENT

The authors declare that they have no competing financial interests.

Received 29 September; accepted 5 October 2004

Published online at <http://www.nature.com/natureneuroscience/>

- Hughes, J.R. *Clin. Electroencephalogr.* **26**, 1–6 (1995).
- Ermentrout, G.B. & Kleinfeld, D. *Neuron* **29**, 33–44 (2001).
- Wheatstone, C. *Philos. Trans. R. Soc. Lond.* **128**, 371–394 (1838).
- Wilson, H.R., Blake, R. & Lee, S.H. *Nature* **412**, 907–910 (2001).
- Wolfe, J.M. *Vision Res.* **24**, 471–478 (1984).
- Heeger, D.J., Huk, A.C., Geisler, W.S. & Albrecht, D.G. *Nat. Neurosci.* **3**, 631–633 (2000).
- Engel, S.A. *et al. Nature* **369**, 525 (1994).
- Logothetis, N.K. & Schall, J.D. Neural correlates of subjective visual perception. *Science* **245**, 761–763 (1989).
- Leopold, D.A. & Logothetis, N.K. *Nature* **379**, 549–553 (1996).
- Sheinberg, D.L. & Logothetis, N.K. *Proc. Natl. Acad. Sci. USA* **94**, 3408–3413 (1997).
- Lumer, E.D., Friston, K.J. & Rees, G. *Science* **280**, 1930–1934 (1998).
- Tong, F., Nakayama, K., Vaughan, J.T. & Kanwisher, N. *Neuron* **21**, 753–759 (1998).
- Tong, F. & Engel, S. *Nature* **411**, 195–199 (2001).
- Polonsky, A., Blake, R., Braun, J. & Heeger, D. *Nat. Neurosci.* **3**, 1153–1159 (2000).
- Lee, S.H. & Blake, R. *J. Vis.* **2**, 618–626 (2002).



Travelling waves of activity in primary visual cortex during binocular rivalry

Sang-Hun Lee, Randolph Blake, and David J. Heeger

Supplementary Methods

Data were acquired from three male observers, 25-34 years old, all with normal or corrected-to-normal vision, on a GE 3 Tesla scanner with a custom dual surface coil (NMSC-002-TR-3GE transmit-receive coil, Nova Medical, Wakefield, MA).

Experiments were carried out with the written consent of each observer, and in compliance with the safety guidelines for MR research, as approved by the Stanford University Panel on Human Subjects in Medical Research. Each observer participated in multiple scanning sessions: one session to obtain a high-resolution anatomical volume, one session to define the early retinotopic visual areas including V1, one session to locate the subregion of each visual area that corresponded to the annulus region in which stimuli were presented, and several fMRI scanning sessions to measure fMRI responses under the various experimental conditions.

Each MR scanning session began by acquiring a set of anatomical images using a T1-weighted SPGR pulse sequence (TR = 10 ms, minimum TE, FA = 15°, 6 NEX, FOV = 220 mm, 3-mm slice thickness) in the same slices as the functional images. The eight oblique slices, roughly perpendicular to the calcarine sulcus, were arranged carefully to encompass the subregion of V1, and other visual areas if possible, that corresponded to the stimulus annulus, which was defined in a separate scanning session (see below). These inplane anatomical images were aligned to a high-resolution anatomical volume of each observer's brain using custom software¹, so that the functional data across multiple scanning sessions from a given observer were coregistered to an accuracy of ~ 1 mm.

Each fMRI scanning session included 8-13 functional scans. During each scan, a time series of fMRI volumes was acquired using a single-shot, T2*-sensitive, spiral-trajectory, gradient-recalled-echo pulse sequence² (TE = 30 ms, TR = 500 ms, FA = 46, FOV = 220 mm, effective inplane pixel size = 3 x 3 mm, 3-mm slice thickness). To minimize head movements, observers were stabilized on a bite bar.

Rival stimuli were a radial grating and a spiral grating, each restricted to an annulus around fixation (spatial frequency = 2.5 cyc/°, radius of annulus center = 4°, width of spiral grating annulus = .8°, Gaussian half-width of radial grating annulus = .4°). The two monocular images were presented on the two halves of a flat-panel display (Multisync LCD 2000, NEC-Mitsubishi, Japan) positioned at the foot of the scanner bed. The display was viewed through binoculars. A pair of angled mirrors, attached to the binoculars, enabled the observer to see the two monocular images. A septum was placed near the observer's knees, and the mirrors were adjusted so that the observer could see only one image in each eye.

Each trial lasted 9 s and consisted of several phases (**Supplementary Fig. 1** online). First, the low-contrast grating was presented to one eye, followed 30 ms later by the high-contrast grating to the other eye. This sequence of events promoted complete perceptual dominance of the high-contrast grating. Shortly (450 ms) thereafter, the contrast in a small region of the low-contrast grating at the top of the annulus was increased briefly (75 ms) and abruptly, then returned to its original low-contrast value. This contrast pulse typically triggered a perceptual travelling wave (**Supplementary Video 1** online). Observers pressed a key when a perceptual wave reached a target area (marked by nonius lines) at the bottom of the annulus. Upon this key press, the two monocular gratings disappeared until the beginning of the next trial.

On a minority of trials (38%), the contrast pulse either failed to evoke a perceptual travelling wave or the travelling wave dissipated somewhere along both paths before reaching the target area. Observers pressed a different key to indicate these failure trials. At all times during the trials, observers maintained strict fixation on the small checkerboard located in the center of the stimulus annulus.

The contrast of the spiral grating was always 100% whereas the contrast of the radial grating was adjusted to achieve two goals simultaneously: i) to maximize the number of trials in which perceptual travelling waves were experienced and ii) to maximize the difference in contrast between the spiral and the radial grating. To do this, the contrast level of the radial grating was adjusted throughout each scanning session. At the beginning of each session, we chose the initial contrast level based on a psychophysical test, which determined the contrast level at which the observer perceived travelling waves most frequently. During the first scan, the contrast of the radial grating slightly varied around the initial contrast level. In the following scan, the contrast varied around a new level, at which waves were experienced most frequently in the previous scan. This contrast adjustment was repeated throughout each session.

The fMRI data were analyzed as follows. First, we discarded the first 9 seconds of data from each scan to minimize the effects of transient magnetic saturation. Second, any residual head movements within each scan and across scans were corrected using custom software¹. Third, the time series from each slice was interpolated (linear interpolation) and shifted in time to compensate for the differential slice acquisition times. Fourth, the time series at each voxel was high-pass filtered to compensate for the slow signal drift in the fMRI signals. Fifth, the time series at each voxel was divided by its mean intensity to convert the data from arbitrary image intensity units to percent

signal modulation and to compensate for the decrease in mean image intensity with distance from the receive coil.

The resulting time series were analyzed for gray matter voxels in each visual area that corresponded retinotopically to the stimulus annulus. These voxels were identified separately for each observer in four steps. First, the retinotopically organized visual areas were identified, following well-established methods, by measuring polar angle and eccentricity components of the cortical retinotopy map³⁻⁶. Second, a subset of voxels in these visual areas that corresponded to the cortical representation of the stimulus annulus was selected based on a separate series of reference scans. During these reference scans, observers held fixation while the display alternated every 9.4 s between a high-contrast checkerboard within the stimulus annulus and its geometric complement, a checkerboard pattern everywhere except the annulus. Data were averaged across six to ten repeated scans, each with eleven cycles of alternations. Voxels were included in the analysis only if they were strongly correlated ($r > .6$ and 0-6 time lag) with the stimulus alternations. Third, the selected voxels were further restricted according to two localizer scans, one at the start and the other at the end of each scanning session. During these localizer scans, the display alternated between a high-contrast checkerboard within the stimulus annulus and a uniform gray field of the same mean luminance. We chose the subset of voxels that were correlated ($r > .7$) with the stimulus alternations in both of the reference scans. This was done because a portion of the session-to-session variability in fMRI responses derives from small differences in slice orientation and position such that voxels which were mostly gray matter in one session are only partially gray matter in a subsequent session. We have found that a within-session localizer can effectively compensate for this source of variability,

leading to noticeable improvement in the session-to-session reliability of the measurements. Fourth, for each voxel, we estimated the distance on the flattened cortical surface from the cortical representation of the top of the annulus based on its polar angle measurement from the retinotopy session. Cortical distances were measured in the 3D cortical manifold (the boundary between white matter and gray matter) using custom software⁷. We discarded voxels that represented the visual field within 30° on either side of the upper vertical meridian, where the trigger was presented, because fMRI responses at those voxels were likely to be contaminated by the physical contrast increment.

fMRI response amplitudes and temporal delays were computed as follows. The measured time series for each of the identified gray matter voxels was averaged across trials. This averaged time series was then fitted using a sinusoidal function. The best-fit sinusoid provided a continuous description of the time series. The temporal delay (time-to-peak) and response amplitude of the fMRI responses were estimated as the phase and amplitude, respectively, of the best-fit sinusoid. Correlations between temporal delay and distance (Fig. 1c) were computed using linear regression. The Pearson χ^2 test was used to determine whether correlation values were significantly different from zero. Previous measurements in our lab have indicated modest spatial correlations in the noise in our fMRI measurements such that the data are over-sampled by a factor of ~4, i.e., by a factor of 2 in each of the 2 image dimensions (unpublished observations). In performing the chi-square test, therefore, the number of degrees of freedom was reduced by a factor of 4 to compensate for the existence of correlated noise in adjacent voxels.

Error estimates for the statistical test of slopes and y-intercepts in Fig 1c were obtained with a bootstrap method⁸ in which random picks (with replacement) were

repeatedly taken from the experimentally obtained data sets, separately for each speed condition (slow, medium, fast). The means and standard errors of slopes and y-intercepts were then computed from 1000 samples of these synthetic data, thus generating bootstrap estimates of the sampling distributions.

The latencies of the underlying neural activity at each voxel (Fig. 1d) were estimated from the fMRI responses by adopting a model of the neural activity and a model of the hemodynamics:

$$r(t) = h(t) * n(t)$$

where $r(t)$ is the fMRI response, $h(t)$ is the hemodynamic impulse response, $n(t)$ is the neural activity, and $*$ represents convolution¹⁰. The underlying neuronal activity at each voxel, $n(t)$, was assumed to go through four states during each trial: a transient response to the onset of stimulus (assumed to last for 200 ms), a sustained response to the higher contrast, a sustained response to the lower stimulus contrasts, and no response while the display was blank (uniform gray) during the inter-trial interval. These four states were characterized by two parameters: the amplitude of the transient response (R_t), and the ratio of the responses to the high and low contrasts (R_c). The hemodynamic impulse response was modeled as:

$$h(t) = \exp(-t/\tau_1) \sin(2\pi f_1 t) - a \exp(-t/\tau_2) \sin(2\pi f_2 t).$$

We have found in previous work⁹ (D. Ress, B.T. Backus & D.J. Heeger, *Soc. Neurosci. Abstr.*, 2000) that this functional form is a better fit to the hemodynamics than the commonly used Gamma function¹⁰. The parameters τ_2 and f_2 were set to 7.4 s and 0.12 Hz, respectively, based on previous measurements in our lab⁹ (D. Ress, B.T. Backus & D.J. Heeger, *Soc. Neurosci. Abstr.*, 2000). The remaining parameters (R_t , R_c , τ_1 , f_1 , a)

were determined separately for each observer by fitting the data from the replay/physical wave experiment. Specifically, the model was chosen to fit simultaneously the measured fMRI responses from four subregions of V1 gray matter (each corresponding to a 30° segment of the stimulus annulus from a quadrant of the visual field). Note that we had complete information about the timing of neural events during replay; only the neural response amplitudes and hemodynamic parameters were determined by fitting the model. The model accounted for 94% of the variance in the measured fMRI responses in V1 during replay, for each of the 3 observers. The best-fit parameters were comparable across the 3 observers ($R_t=0.5-0.75$; $R_c=5.5-8.0$; $\tau_1=6.5-7.0$; $f_1=0.35-0.65$; $a=0.08-0.1$).

The model was then used, with the model parameters fixed, to estimate the latencies of the underlying neural activity during rivalry. This was complicated by the fact that the contrast pulse failed to evoke complete perceptual travelling waves on some trials (see above). Because we did not know exactly what happened on each such failure trial, and because the failure trials were interleaved with the valid trials, we could not perform a straightforward least-squares fit to the measured time series. Instead, we used the model to generate simulated fMRI responses (response amplitudes and temporal delays) which were used as lookup tables to determine the neural latencies. Specifically, we simulated 100 scans for each observer, resulting in about 1000 ~ 1500 complete travelling waves (assumed to propagate at constant velocity) interleaved with a number of failure trials (matching the proportion of failures reported by each observer). The model response amplitudes and temporal delays were extracted from these simulations, following the steps that were used to analyze the real fMRI data. This resulted in a lookup table for each observer which associated the temporal latency of the

underlying neural activity with a corresponding fMRI response amplitude and temporal delay. Finally, we used the lookup tables to determine the neural latencies associated with simulated response amplitudes and delays that best matched the measured response amplitudes and delays.

References

1. Nestares, O. & Heeger, D. J. Robust multiresolution alignment of MRI brain volumes. *Magn. Reson. Med.* **43**, 705-715 (2000).
2. Glover, G. H. Simple analytic spiral K-space algorithm. *Magn. Reson. Med.* **42**, 412-415 (1999).
3. Engel, S. A., Rummelhart, D. E., Wandell, B. A., Lee, A. T., Glover, G. H., Chichilnisky, E. J. and Shadlen, M. N. fMRI of human visual cortex. *Nature* **369**, 525. (1994).
4. Sereno, M. I., Dale, A. M., Reppas, J. B., Kwong, K. K., Belliveau, J. W., Brady, T. J., Rosen, B. R. & Tootell, R. B. Borders of multiple visual areas in humans revealed by functional magnetic resonance imaging. *Science* **268**, 889-893 (1995).
5. DeYoe, E. A., Bandettini, P., Neitz, J., Miller, D. & Winans, P. Functional magnetic resonance imaging (fMRI) of the human brain. *J. Neurosci. Methods* **54**, 171-187 (1994).
6. Engel, S. A., Glover, G. H. & Wandell, B. A. Retinotopic organization in human visual cortex and the spatial precision of functional MRI. *Cereb. Cortex* **7**, 181-192 (1997).
7. Dougherty, R. F., Koch, V. M., Brewer, A. A., Fischer, B., Modersitzki, J. & Wandell, B. A. Visual field representations and locations of visual areas V1/2/3 in human visual cortex. *J. Vis.* **3**, 586-598 (2003).

8. Efron, B. & Tibshirani, R. *An introduction to the bootstrap*. (Chapman & Hall, New York, 1993).
9. Polonsky, A., Blake, R., Braun, J. & Heeger, D. Neural activity in human primary visual cortex correlates with perception during binocular rivalry. *Nature Neurosci.* **3**, 1153–1159 (2000).
10. Boynton, G. M., Engel S. A., Glover, G. H. & Heeger, D. J. Linear systems analysis of functional magnetic resonance imaging in human V1. *J. Neurosci.* **16**, 4207-4221 (1996).